PROCEEDINGS OF SCIENCE

Sensitivity of the IceCube-Gen2 Surface Array for Cosmic-Ray Anisotropy Studies

The IceCube-Gen2 Collaboration
(a complete list of authors can be found at the end of the proceedings)

E-mail: wenjie.hou@kit.edu

The energy of the transition from Galactic to extra-galactic origin of cosmic rays is one of the major unresolved issues of cosmic-ray physics. However, strong constraints can be obtained from studying the anisotropy in the arrival directions of cosmic rays. The sensitivity to cosmic-ray anisotropy is, in particular, a matter of statistics. Recently, the cosmic ray anisotropy measurements in the TeV to PeV energy range were updated from IceCube using 11 years of data. The IceCube-Gen2 surface array will cover an area about 8 times larger than the existing IceTop surface array with a corresponding increase in statistics and capability to investigate cosmic-ray anisotropy with higher sensitivity. In this contribution, we present details on the performed simulation studies and sensitivity to the cosmic-ray anisotropy signal for the IceCube-Gen2 surface array.

Corresponding authors: Wenjie Hou[1*]
[1] *Karlsruhe Institute of Technology (KIT), Institute for Astroparticle Physics, D-76021 Karlsruhe, Germany*

[*] Presenter

The 38th International Cosmic Ray Conference (ICRC2023)
26 July – 3 August, 2023
Nagoya, Japan

PoS(ICRC2023)354

1. Introduction

One of the most significant unresolved questions in cosmic ray (CR) physics pertains to the energy at which the transition from Galactic to extragalactic cosmic rays occurs. This transition holds the key to understanding some of the issues regarding the origin of CRs, as it is believed to mark the point where the sources of CRs shift from the Milky Way to extragalactic systems. Pinpointing the exact energy of this transition remains a challenge, as the trajectories of CRs are significantly influenced by the magnetic fields present in the Galaxy, making it difficult to trace individual CRs back to their specific origins.

However, constraints can be obtained by studying the large-scale anisotropy in the CR arrival directions. In the past few decades, several experiments have provided long-term and significant observations of a subtle sidereal anisotropy across a wide energy range from 1 TeV to 100 EeV. These ground-based experiments, located in both the northern and southern hemispheres, have detected large-scale anisotropy in CRs with a high level of statistical significance [1–13]. The magnitude of the observed large-scale anisotropy, ranging from 10^{-4} to 10^{-2}, combined with its energy dependence and angular structure, hints at changes in the origin of the CRs versus energy.

However, statistically significant measurements of the projected dipole amplitude are missing in the energy range between 2 PeV and 8 EeV. The Pierre Auger Observatory has not yet observe a significant dipole below 8 EeV [12], and KASCADE-Grande did not find evidence for a dipole anisotropy in the data with median energy from 2.7 PeV to 33 PeV [2, 14]. Therefore, both collaborations set upper limits at 99% confidence on the reconstructed (projected) dipole. IceCube-Gen2, along with its surface array, will be capable of filling a portion of the energy gap between 1 PeV and approximately 100 PeV.

IceCube-Gen2, the next generation of the IceCube Neutrino Observatory [15], will be located at the South Pole with a mission to detect high-energy and ultra-high energy cosmic rays and neutrinos, study hadronic interactions, and contribute to the broader field of astroparticle physics. It will incorporate three detector arrays: a deep optical array, a radio array, and a hybrid surface array [16]. The hybrid surface array combines scintillator panels and radio antennas in surface stations. Currently, the IceCube-Gen2 surface array is in the stage of technical design, but CORSIKA simulations of air shower detection have already been performed [16].

Here, we present the air shower reconstruction efficiency for the scintillators of the IceCube-Gen2 surface array, describe the Monte Carlo studies of the CR arrival directions and show the sensitivity of the surface array to large-scale anisotropy of the CRs based on simulated events.

2. Reconstruction efficiency of IceCube-Gen2 surface array

The planned surface area covered by the IceCube-Gen2 surface array is 6.6 km^2 (depends on the definition of the containment cuts). The corresponding CORSIKA simulations of the scintillator array response were performed for proton- and iron- induced air showers with $4 \leq \log_{10}(E/\mathrm{GeV}) \leq 8$ and zenith angles (θ) up to 51°, and $4 \leq \log_{10}(E/\mathrm{GeV}) \leq 7.5$ with θ up to 63° [16]. To simulate a large sample of contained events, the shower cores were randomly distributed within a 1.5 km radius from the center of the surface array. The detector response was then simulated for the scintillators, where the secondary particles on the ground were injected into the scintillator panels.

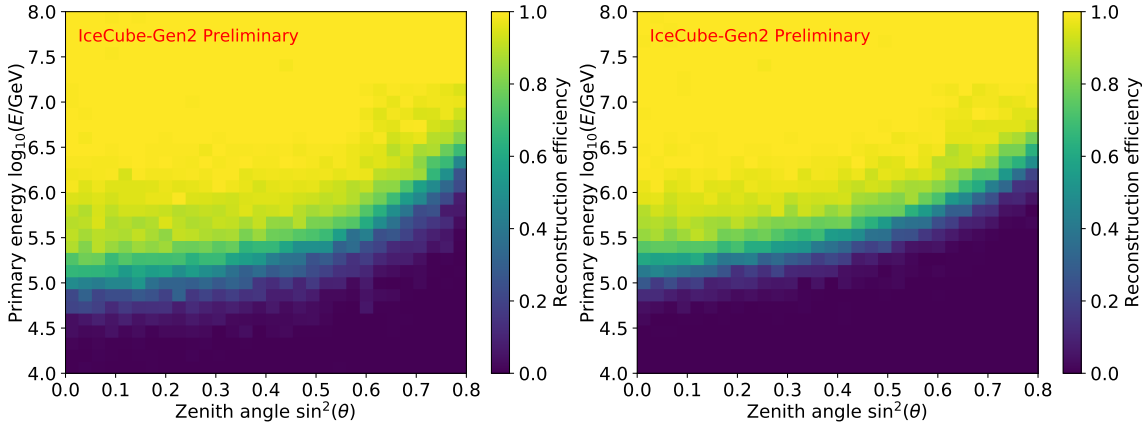

Figure 1: 2D histograms of the reconstruction efficiency for proton- (left) and iron- (right) induced air shower for scintillators in the IceCube-Gen2 surface array, with energy range from 10^6 GeV to 10^8 GeV, zenith angle up to 63° in $\sin^2\theta$ scale, and scintillator multiplicity ≥ 5 to trigger the event.

To show realistic capabilities of the IceCube-Gen2 surface array, we perform a selection process that involves choosing true air shower core locations (x, y) within a distance of 100 meters from the polygonal edge of the array taking into account the air shower footprints. The scintillator array is fully efficient (100%) in triggering on air showers above 0.5 PeV for vertical events ($\theta = 0$). Considering the scintillator triggered multiplicities ≥ 5, we show the reconstruction efficiencies for proton and iron primaries and make the histograms for these two CR primary particles, fill in the missing region $0.6 \leq \sin^2(\theta) \leq 0.8$ and $7.5 \leq \log_{10}(E/\mathrm{GeV}) \leq 8$ assuming a 100% efficiency (see Figure 1), and fit the unbroken histograms with a modified error function (2 dimensional) as a function of the energy E and the zenith angle with $z = \sin^2\theta$:

$$\epsilon(E, z) = \frac{1}{2}\left[1 + \mathrm{erf}\left(\frac{E - (\mu_0 + \mu_1 z + \mu_2 z^2 + \mu_3 z^3)}{\sigma_0 + \sigma_1 z}\right)\right]. \tag{1}$$

The parameters for both proton and iron in Eq.(1) are listed in Table 1. We estimate the reconstruction efficiencies for helium, nitrogen, and aluminum using the natural logarithm of their mass number, denoted as $\ln A$. This estimation is based on the logarithmic mass dependence of the cosmic-ray primaries. The reconstruction efficiency for helium, nitrogen, and aluminum can be written as

$$\epsilon(A_i, E, z) = \frac{\ln A_i}{\ln A_{\mathrm{Fe}} - \ln A_{\mathrm{P}}}\left[\epsilon_{\mathrm{Fe}}(E, z) - \epsilon_{\mathrm{P}}(E, z)\right] + \epsilon_{\mathrm{P}}(E, z), \tag{2}$$

where i ranges from 1 to 3, representing the estimated helium, nitrogen, and aluminum, respectively. The contour lines represent 50% and 98% of the reconstruction efficiency using Eq.(1), as shown

Particle	μ_0	μ_1	μ_2	μ_3	σ_0	σ_1
Proton	5.017 ± 0.008	0.711 ± 0.083	-1.791 ± 0.240	3.824 ± 0.198	0.483 ± 0.008	0.001 ± 0.000
Iron	5.177 ± 0.006	0.753 ± 0.063	-0.665 ± 0.182	2.073 ± 0.149	0.404 ± 0.006	-0.067 ± 0.012

Table 1: Parameters in the fit function (1) of cosmic ray reconstruction efficiency of the IceCube-Gen2 surface array. Only proton and iron are covered in this table.

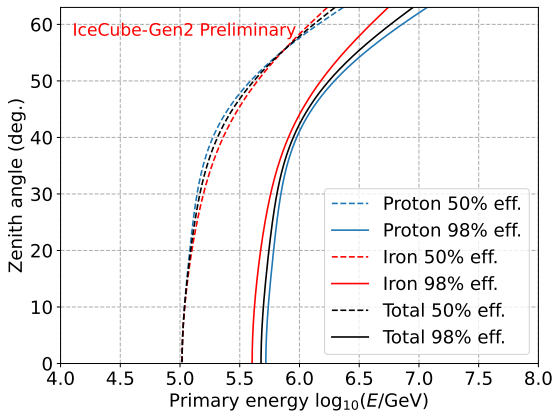

Figure 2: Contour lines with 50% and 98% reconstruction efficiency of the IceCube-Gen2 surface array are shown for proton and iron, The total efficiency of all particles utilizes the H4a flux model [18].

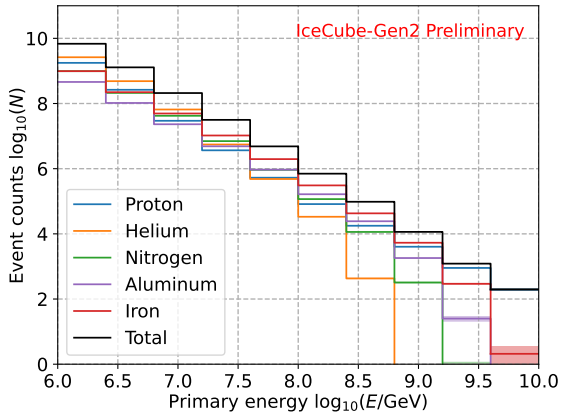

Figure 3: Histogram of the event counts of the IceCube-Gen2 surface array with a 10-year exposure, considering the H4a flux model and the reconstruction efficiency with 3 additional energy bins.

in Figure 2. The total efficiency of all particles utilizes Eq.(1), (2) and the H4a flux model [17].

The scintillators will be the most sensitive component of the surface hardware of IceCube-Gen2 and thereby determine the energy threshold necessary for cosmic-ray detection. In the resolution analysis of the reconstructed arrival direction [16] it is observed that, at threshold energies of approximately 1 PeV, the direction can be reconstructed with an accuracy of a few degrees for air showers with zenith angles up to 45°. Above 10 PeV the angular resolution reaches the sub-degree level. The accurate estimation of the shower geometry and the reliable determination of the arrival direction make it highly valuable for studying cosmic-ray anisotropy.

3. Monte-Carlo simulation of cosmic-ray arrival directions

We now apply the reconstruction efficiency to simulate the arrival directions for the IceCube-Gen2 surface array with a 10-year exposure. The simulation is divided into 7 energy bins ranging from 10^6 GeV to $10^{8.8}$ GeV with a bin size of 0.4 in $\log_{10}(E/\mathrm{GeV})$. In each energy bin, we inject 15 different dipoles at declinations ranging from −80° to 80°. In total, we have 1785 injected dipoles and their corresponding sky maps. To get a precise and stable value of the reconstructed dipole amplitude we choose dipole amplitudes depending on the declination, focusing on amplitudes that can be detected at $> 10\sigma$ within 10 years of operation. Otherwise, it would be required to simulate the same dipole repeatedly to adequately capture the uncertainties.

Using the H4a flux model [17], the number of arrival directions in each energy bin can be calculated by integrating the 2D function in Eq.(1) and (2) of reconstruction efficiency and the number of cosmic rays with 10 years of exposure of the IceCube-Gen2 surface array. This calculation is a function of E and z. Therefore, we have the event counts for each of the 5 primary components in the energy bins (see Figure 3):

$$N_{\mathrm{eff},ij} = \int_{\theta_{\min}}^{\theta_{\max}} \int_{E_{j-1}}^{E_j} \epsilon_i\,(E,\theta)\, N_{\mathrm{H4a},i}\,(E)\, dE\, d\theta, \tag{3}$$

where i ranges from 1 to 5 for the 5 primary particles, j ranges from 1 to 8 for the edges of the 7 energy bins, and $N_{\mathrm{H4a},i}$ represents the event counts for each of the 5 primary particles using the H4a flux model. In total, we have 8.355 billion simulated cosmic ray events over all 7 energy bins. Taking into account the ratio of different primaries weighted by the mass-dependent H4a flux expressions [17] and Eq.(1) and (2), the total efficiency averaged over all primaries is written as

$$\epsilon_{\mathrm{tot}}\left(E,\theta\right)=\frac{\Sigma_{i=1}^{5}\epsilon_i\left(E,\theta\right)\phi_{\mathrm{H4a},i}\left(E\right)}{\Sigma_{i=1}^{5}\phi_{\mathrm{H4a},i}\left(E\right)}. \tag{4}$$

Next, we randomly inject the CR arrival directions using relative acceptance of the detector for all energy bins and all zenith angles below threshold and scan over the dipole declination from $-80°$ to $80°$ with bin size of $10°$. The amplitudes are chosen from 7×10^{-3} up to 9.56×10^{-1} for the injected dipole with different energy bins covering different ranges of the amplitude. The distribution function of the CRs is a function of exposure of the IceCube-Gen2 surface array,

$$\omega_{\mathrm{Gen2}}\left(E,\theta,\theta_{\mathrm{max}},\mathcal{A},\delta_{\mathrm{d}},\delta_{\mathrm{Gen2}}\right)=\omega\left(\theta,\theta_{\mathrm{max}},\delta_{\mathrm{Gen2}}\right)\times\epsilon_{\mathrm{tot}}\left(E,\theta\right)\times\mathcal{D}\left(\mathcal{A},\delta_{\mathrm{d}},\delta_{\mathrm{Gen2}}\right), \tag{5}$$

where δ_{d} denotes the dipole declination, ω is the relative exposure of an observatory at declination $\delta_{\mathrm{Gen2}}=-89.99°$ without detector efficiencies. The function $\mathcal{D}\left(\mathcal{A},\delta_{\mathrm{d}},\delta_{\mathrm{Gen2}}\right)$ provides the dipole distribution, taking into account the relative orientation of the IceCube-Gen2 surface array to the dipole.

4. Sensitivity to the cosmic ray anisotropy

To assess the sensitivity of a partial-sky coverage observatory to a dipole anisotropy, it is essential to compare the actual sky map of injected CR arrival directions (data map with simulated dipole in Eq.(5)) with a sky map that reflects the detector's response to a isotropic CR flux (reference map without dipole). Note that the reference map, with dipole distribution function $\mathcal{D}\left(\mathcal{A},\delta_{\mathrm{d}},\delta_{\mathrm{Gen2}}\right)=1$, is not itself isotropic. This comparison allows us to evaluate the deviation from isotropy and quantify the presence of the dipole anisotropy in the simulated data by Eq.5. Therefore, the residual between the data maps and the reference maps, which are obtained by normalizing each declination band independently, is sensitive only to anisotropy in right ascension (α). In particular, the fitting of the dipole's projection in the equatorial plane with the first harmonic allows for a direct measurement of a dipolar cosmic ray distribution.

Based on the Monte-Carlo simulation as described in §3, we generate sky maps of relative intensity $I=(N_{\mathrm{pix},i}-\langle N\rangle_{\mathrm{pix},i})/\langle N\rangle_{\mathrm{pix},i}$, where $N_{\mathrm{pix},i}$ represents the data map while $\langle N\rangle_{\mathrm{pix},i}$ represents the background map. Then, we perform a one-dimensional (1D) projection of the sky map and fit it with a first harmonic function $\mathcal{A}_{\mathrm{reco}}\cos\left(n(\alpha-\phi)\right)+B$, where $\mathcal{A}_{\mathrm{reco}}$ is the amplitude of the reconstructed dipole, ϕ is the phase, and B is a constant. The reconstruction ratio $\mathcal{A}_{\mathrm{reco}}/\mathcal{A}$ in the majority of the cases are below 80% due to the limited field of view (FoV) of the surface array.

To assess the significance of a dipole deviation from isotropy, we consider a null hypothesis in number of sigmas $n_\sigma=\left(\mathcal{A}_{\mathrm{reco}}-\mathcal{A}_{\mathrm{hypo}}\right)/\sigma_{\mathcal{A}}$, where $\mathcal{A}_{\mathrm{hypo}}$ is set to 0, representing the expected value under the null hypothesis (different from the full-sky case [18]). We assume that the $\sigma_{\mathcal{A}}$ of the dipole amplitude reconstruction is proportional to $1/\sqrt{N}$ verified through both Monte Carlo

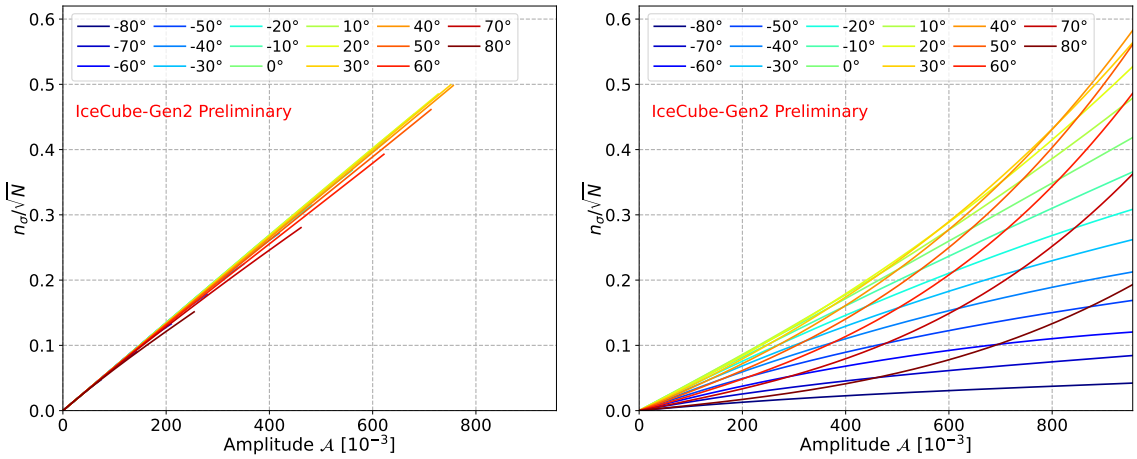

Figure 4: The fitting curves of the reconstructed dipole (left) and the corresponding true dipole (right) are shown based on the sampled data points $(n_\sigma/\sqrt{N}, \mathcal{A})$ obtained from the simulation in Section 3.

simulation and the covariance matrix in the first harmonic fit of the 1D projected map. Therefore, the sensitivity function (number of sigmas) can be expressed as follows:

$$n_\sigma = \mathcal{S}\left(\mathcal{A}, E, \theta_{\max}, \delta_{\mathrm{d}}, \delta_{\mathrm{Gen2}}\right) \mathcal{A}\sqrt{N}, \tag{6}$$

where $\mathcal{S}$ is defined as a sensitivity coefficient. We need to clarify that the sensitivity to the true dipole, denoted as $n_\sigma = \mathcal{S}_{\mathrm{true}}\mathcal{A}_{\mathrm{true}}\sqrt{N}$, is not obtained directly from the reconstruction of the true dipole (or input dipole $\mathcal{A}$). Instead, it represents the corresponding true dipole of the 3σ or 5σ reconstructed dipole, denoted as $n_\sigma = \mathcal{S}_{\mathrm{reco}}\mathcal{A}_{\mathrm{reco}}\sqrt{N}$, which will be obtained from the observation by the IceCube-Gen2 surface array in the future. We scatter the data points $(n_\sigma/\sqrt{N}, \mathcal{A})$ for both the reconstructed dipole and true dipole cases and fit these data points with a polynomial equation of the form $\Sigma_{i=1}^{3}\lambda_i\mathcal{A}^i$, where λ_i are the coefficients of the polynomial (see Figure 4). The slope of these curves represents the sensitivity coefficients for both the reconstructed and true dipole cases.

$$\mathcal{S}(\mathcal{A}, E) = \lambda_1(E) + 2\lambda_2(E)\mathcal{A} + 3\lambda_3(E)\mathcal{A}^2. \tag{7}$$

where λ_1, λ_2, λ_3, are different parameters for proton and iron which are energy dependent. Figure 5 shows the ratio between the reconstructed dipole and the true dipole. The sensitivity curves and bands for both 3σ and 5σ are shown in Figure 6, the corresponding points are in Table 2.

Median energy E_i	1.8 PeV	4.4 PeV	11 PeV	28 PeV	70 PeV	176 PeV	441 PeV
$\mathcal{A}_{\mathrm{reco}}$ ($\times 10^{-3}$) 3σ	0.0865	0.1991	0.4934	1.2723	3.2468	8.5073	22.9160
	0.4998	1.1515	2.8600	7.4196	19.2255	52.6080	163.7749
$\mathcal{A}_{\mathrm{reco}}$ ($\times 10^{-3}$) 5σ	0.1441	0.3318	0.8222	2.1203	5.4098	14.1687	38.0990
	0.8334	1.9210	4.7783	12.4455	32.5946	92.2597	341.6183
$\mathcal{A}_{\mathrm{true}}$ ($\times 10^{-3}$) 3σ	0.5442	1.2528	3.1048	8.0071	20.4322	53.5486	144.4248
$\mathcal{A}_{\mathrm{true}}$ ($\times 10^{-3}$) 5σ	0.9071	2.0880	5.1744	13.3435	34.0472	89.2095	241.9074

Table 2: Points of the 3σ and 5σ sensitivity bands for the reconstructed dipole for each energy bin E_i ($i = 1$ to 7), upper and lower boundary of the corresponding true dipole for both cases (sensitivity bands).

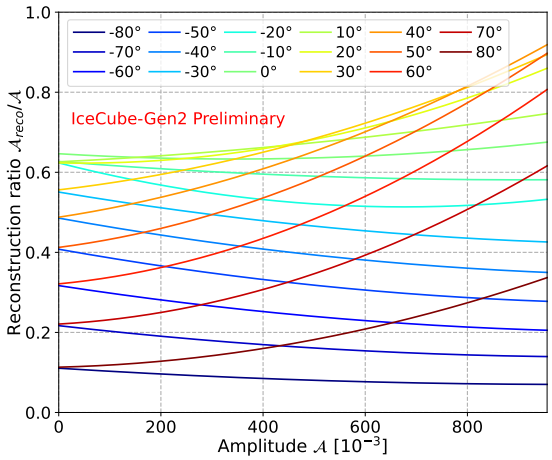

Figure 5: Ratio between reconstructed dipole and true dipole in the Monte-Carlo simulation. The amplitudes are chosen from 7×10^{-3} up to 9.56×10^{-1} for the true dipole. However, different energy bins cover different ranges of the true dipole amplitude. The curves show the propagation of the ratio with the declination of the true dipole from -80 degree to 80 degree with angle bin size of 10 degree.

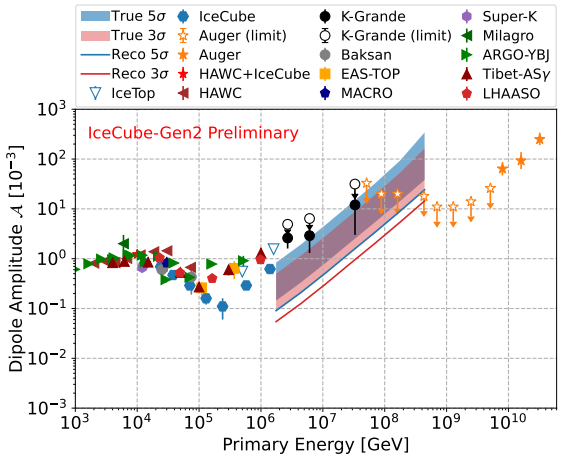

Figure 6: The curves show the 3σ and 5σ sensitivity of the IceCube-Gen2 surface array to the reconstructed dipole, bands show the corresponding true dipole of the 3σ and 5σ reconstructed dipole. The data points shown are reconstructed dipole amplitudes from the various experiments [1–13]. The upper limits of KASCADE-Grande and Auger are from 2.7 PeV to 8 EeV, where the energy gap exists.

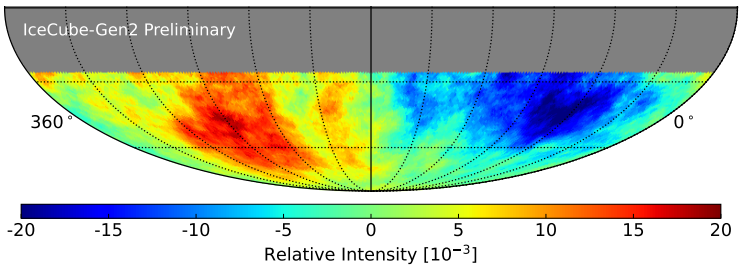

Figure 7: Simulated relative intensity map for IceCube-Gen2 surface array with 5σ of a reconstructed amplitude 9.029×10^{-3} at 176 PeV. The injected dipole orientation is set as $(270°, -10°)$ for the right ascension and declination. The corresponding amplitude of true dipole is 1.437×10^{-2}.

The sensitivity curves of the reconstructed dipole and bands of the corresponding true dipole (full dipole) of the IceCube-Gen2 surface array are shown in Figure 6, which represents the significance of a deviation from the null hypothesis (isotropy). The curves of $\mathcal{A}_{\rm reco}$ are lower than the bands of true amplitude due to the field of view (FoV) of the IceCube-Gen2 surface array. Taking into account the energy gap region with upper limits and the highest energy data from IceCube, the energy range chosen for this work is from 10^6 GeV to the overlap region with Auger, approximately around $10^{8.8}$ GeV. A dipole with a very inclined orientation is difficult to reconstruct using the 1D projection method. Thus, IceCube-Gen2 will need to be combined with experiments on the norther hemisphere (e.g. IceCube [11], HAWC [1]). Moreover, it is necessary to consider very inclined dipole declinations, due to the lack of information on dipole declination from existing data.

By considering Eq. (6) and (7), we also plot the sky map of relative intensity at 176 PeV with

an assumed 5σ significance level for the reconstructed dipole with amplitude of 9.029×10^{-3}, and with 20° top hat smoothing. The dipole orientation is set as $(270°, -10°)$ for the right ascension and declination. The corresponding amplitude of the injected true dipole ($\mathcal{A} = 1.437 \times 10^{-2}$) can be derived using the reconstruction ratio $\mathcal{A}_{\rm reco}/\mathcal{A}$. We use HEALPix (with Nside = 64) for the sky map, the size of each pixel tile in the sky map is approximately $(0°.84)^2$.

5. Conclusion and outlook

We present the 2D function of the air shower reconstruction efficiency of proton and iron primaries for the IceCube-Gen2 surface array based on the existing CORSIKA simulation, estimate the reconstruction efficiencies for helium, nitrogen, and aluminum using the natural logarithm of their mass numbers and show the total efficiencies of all particles utilizing the H4a flux model. Next, we simulate the CR arrival directions for the surface array using Monte-Carlo simulation by injecting 15 different dipoles at declinations ranging from −80° to 80° for 7 energy bins, which range from 10^6 GeV to $10^{8.8}$ GeV with a bin size of 0.4 in $\log_{10}(E/\text{GeV})$. In total, we have 1785 injected dipoles. In order to study the anisotropy, we compare the actual sky map of an injected dipole with a reference map without a dipole for all 1785 cases, make the sky maps of relative intensity and perform 1D projections of the sky maps and fit them with first harmonic functions. To assess the sensitivity of IceCube-Gen2 surface array to a dipole anisotropy, we consider a null hypothesis and the propagation of the sigmas. Finally, we get the sensitivity function and show the 3σ and 5σ sensitivity to the CR dipole anisotropy with curves and bands for the surface array.

In order to improve the accuracy of the sensitivity analysis for the IceCube-Gen2 surface array, we will extend the threshold of the zenith angle in the CORSIKA simulation up to 80 degrees, which can provide a more accurate estimation of the reconstruction efficiency.

References

[1] **HAWC** Collaboration, A. U. Abeysekara *et al.* *Astrophys.J.* **865** no. 1, (2018) 57.
[2] **KASCADE-Grande** Collaboration, A. Chiavassa *et al.* *PoS* **ICRC2015** (2015) 281.
[3] **Baksan** Collaboration, V. V. Alekseenko *Bull.Russ.Acad.Sci.Phys.* **73** no. 5, (2009) 571–573.
[4] **EAS-TOP** Collaboration, M. Aglietta *et al.* *Astrophys.J.Lett.* **692** (2009) 130–133.
[5] **MACRO** Collaboration, M. Ambrosio *et al.* *Phys.Rev.D* **67** (2003) 042002.
[6] **Super-Kamiokande** Collaboration, G. Guillian *et al.* *Phys.Rev.D* **75** (2007) 062003.
[7] **Milagro** Collaboration, A. A. Abdo *et al.* *Astrophys.J.* **798** (2009) 2121–2130.
[8] **Argo-YBJ** Collaboration, B. Bartoli *et al.* *Astrophys.J.* **809** no. 1, (2015) 90.
[9] **Tibet** Collaboration, M. Amenomori *et al.* *Astrophys.J.Lett.* **626** (2005) 29–32.
[10] **IceCube** Collaboration, M. G. Aartsen *et al.* *Astrophys.J.* **765** (2013) 55.
[11] **IceCube** Collaboration, M. G. Aartsen *et al.* *Astrophys.J.* **826** no. 2, (2016) 220.
[12] **Pierre Auger** Collaboration, A. Aab *et al.* *Astrophys.J.* **891** (2020) 142.
[13] **LHAASO** Collaboration, W. Gao *PoS* **ICRC2021** (2021) 351.
[14] **KASCADE-Grande** Collaboration, A. Chiavassa *et al.* *Astrophys.J.* **870** no. 2, (2019) 91.
[15] **IceCube-Gen2** Collaboration, M. G. Aartsen *et al.* *J.Phys.G* **48** no. 6, (2021) 060501.
[16] **IceCube-Gen2** Collaboration *PoS* **ICRC2021** (2021) 411.
[17] T. K. Gaisser *Astropart. Phys.* **35** (2012) 801–806.
[18] P. Sommers *Astropart. Phys.* **14** (2001) 271–286.

Full Author List: IceCube-Gen2 Collaboration

R. Abbasi[17], M. Ackermann[76], J. Adams[22], S. K. Agarwalla[47, 77], J. A. Aguilar[12], M. Ahlers[26], J.M. Alameddine[27], N. M. Amin[53], K. Andeen[50], G. Anton[30], C. Argüelles[14], Y. Ashida[64], S. Athanasiadou[76], J. Audehm[1], S. N. Axani[53], X. Bai[61], A. Balagopal V.[47], M. Baricevic[47], S. W. Barwick[34], V. Basu[47], R. Bay[8], J. Becker Tjus[11, 78], J. Beise[74], C. Bellenghi[31], C. Benning[1], S. BenZvi[63], D. Berley[23], E. Bernardini[59], D. Z. Besson[40], A. Bishop[47], E. Blaufuss[23], S. Blot[76], M. Bohmer[31], F. Bontempo[35], J. Y. Book[14], J. Borowka[1], C. Boscolo Meneguolo[59], S. Böser[48], O. Botner[74], J. Böttcher[1], S. Bouma[30], E. Bourbeau[26], J. Braun[47], B. Brinson[6], J. Brostean-Kaiser[76], R. T. Burley[2], R. S. Busse[52], D. Butterfield[47], M. A. Campana[60], K. Carloni[14], E. G. Carnie-Bronca[2], M. Cataldo[30], S. Chattopadhyay[47, 77], N. Chau[12], C. Chen[6], Z. Chen[66], D. Chirkin[47], S. Choi[67], B. A. Clark[23], R. Clark[42], L. Classen[52], A. Coleman[74], G. H. Collin[15], J. M. Conrad[15], D. F. Cowen[71, 72], B. Dasgupta[51], P. Dave[6], C. Deaconu[20, 21], C. De Clercq[13], S. De Kockere[13], J. J. DeLaunay[70], D. Delgado[14], S. Deng[1], K. Deoskar[65], A. Desai[47], P. Desiati[47], K. D. de Vries[13], G. de Wasseige[44], T. DeYoung[28], A. Diaz[15], J. C. Díaz-Vélez[47], M. Dittmer[52], A. Domi[30], H. Dujmovic[47], M. A. DuVernois[47], T. Ehrhardt[48], P. Eller[31], E. Ellinger[75], S. El Mentawi[1], D. Elsässer[27], R. Engel[35, 36], H. Erpenbeck[47], J. Evans[23], J. J. Evans[49], P. A. Evenson[53], K. L. Fan[23], K. Fang[47], K. Farrag[43], K. Farrag[16], A. R. Fazely[7], A. Fedynitch[68], N. Feigl[10], S. Fiedlschuster[30], C. Finley[65], L. Fischer[76], B. Flaggs[53], D. Fox[71], A. Franckowiak[11], A. Fritz[48], T. Fujii[57], P. Fürst[1], J. Gallagher[46], E. Ganster[1], A. Garcia[14], L. Gerhardt[9], R. Gernhaeuser[31], A. Ghadimi[70], P. Giri[41], C. Glaser[74], T. Glauch[31], T. Glüsenkamp[30, 74], N. Goehlke[36], S. Goswami[70], D. Grant[28], S. J. Gray[23], O. Gries[1], S. Griffin[47], S. Griswold[63], D. Guevel[47], C. Günther[1], P. Gutjahr[27], C. Haack[30], T. Haji Azim[1], A. Hallgren[74], R. Halliday[28], S. Hallmann[76], L. Halve[1], F. Halzen[47], H. Hamdaoui[66], M. Ha Minh[31], K. Hanson[47], J. Hardin[15], A. A. Harnisch[28], P. Hatch[37], J. Haugen[47], A. Haungs[35], D. Heinen[1], K. Helbing[75], J. Hellrung[11], B. Hendricks[72, 73], F. Henningsen[31], J. Henrichs[76], L. Heuermann[1], N. Heyer[74], S. Hickford[75], A. Hidvegi[65], J. Hignight[29], C. Hill[16], G. C. Hill[2], K. D. Hoffman[23], B. Hoffmann[36], K. Holzapfel[31], S. Hori[47], K. Hoshina[47, 79], W. Hou[35], T. Huber[35], T. Huege[35], K. Hughes[19, 21], K. Hultqvist[65], M. Hünnefeld[27], R. Hussain[47], K. Hymon[27], S. In[67], A. Ishihara[16], M. Jacquart[47], O. Janik[1], M. Jansson[65], G. S. Japaridze[5], M. Jeong[67], M. Jin[14], B. J. P. Jones[4], O. Kalekin[30], D. Kang[35], W. Kang[67], X. Kang[60], A. Kappes[52], D. Kappesser[48], L. Kardum[27], T. Karg[76], M. Karl[31], A. Karle[47], T. Katori[42], U. Katz[30], M. Kauer[47], J. L. Kelley[47], A. Khatee Zathul[47], A. Kheirandish[38, 39], J. Kiryluk[66], S. R. Klein[8, 9], T. Kobayashi[57], A. Kochocki[28], H. Kolanoski[10], T. Kontrimas[31], L. Köpke[48], C. Kopper[30], D. J. Koskinen[26], P. Koundal[35], M. Kovacevich[60], M. Kowalski[10, 76], T. Kozynets[26], C. B. Krauss[29], I. Kravchenko[41], J. Krishnamoorthi[47, 77], E. Krupczak[28], A. Kumar[76], E. Kun[11], N. Kurahashi[60], N. Lad[76], C. Lagunas Gualda[76], M. J. Larson[23], S. Latseva[1], F. Lauber[75], J. P. Lazar[14, 47], J. W. Lee[67], K. Leonard DeHolton[72], A. Leszczyńska[53], M. Lincetto[11], Q. R. Liu[47], M. Liubarska[29], M. Lohan[51], E. Lohfink[48], J. LoSecco[56], C. Love[60], C. J. Lozano Mariscal[52], L. Lu[47], F. Lucarelli[32], Y. Lyu[8, 9], J. Madsen[47], K. B. M. Mahn[28], Y. Makino[47], S. Mancina[47, 59], S. Mandalia[43], W. Marie Sainte[47], I. C. Mariş[12], S. Marka[55], Z. Marka[55], M. Marsee[70], I. Martinez-Soler[14], R. Maruyama[54], F. Mayhew[28], T. McElroy[29], F. McNally[45], J. V. Mead[26], K. Meagher[47], S. Mechbal[76], A. Medina[25], M. Meier[16], Y. Merckx[13], L. Merten[11], Z. Meyers[76], J. Micallef[28], M. Mikhailova[40], J. Mitchell[7], T. Montaruli[32], R. W. Moore[29], Y. Morii[16], R. Morse[47], M. Moulai[47], T. Mukherjee[35], R. Naab[76], R. Nagai[16], M. Nakos[47], A. Narayan[51], U. Naumann[75], J. Necker[76], A. Negi[4], A. Nelles[30, 76], M. Neumann[52], H. Niederhausen[28], M. U. Nisa[28], A. Noell[1], A. Novikov[53], S. C. Nowicki[28], A. Nozdrina[40], E. Oberla[20, 21], A. Obertacke Pollmann[16], V. O'Dell[47], M. Oehler[35], B. Oeyen[33], A. Olivas[23], R. Ørsøe[31], J. Osborn[47], E. O'Sullivan[74], L. Papp[31], N. Park[37], G. K. Parker[4], E. N. Paudel[53], L. Paul[50, 61], C. Pérez de los Heros[74], T. C. Petersen[26], J. Peterson[47], S. Philippen[1], S. Pieper[75], J. L. Pinfold[29], A. Pizzuto[47], I. Plaisier[76], M. Plum[61], A. Pontén[74], Y. Popovych[48], M. Prado Rodriguez[47], B. Pries[28], R. Procter-Murphy[23], G. T. Przybylski[9], L. Pyras[76], J. Rack-Helleis[48], M. Rameez[51], K. Rawlins[3], Z. Rechav[47], A. Rehman[53], P. Reichherzer[11], G. Renzi[12], E. Resconi[31], S. Reusch[76], W. Rhode[27], B. Riedel[47], M. Riegel[35], A. Rifaie[1], E. J. Roberts[2], S. Robertson[8, 9], S. Rodan[67], G. Roellinghoff[67], M. Rongen[30], C. Rott[64, 67], T. Ruhe[27], D. Ryckbosch[33], I. Safa[14, 47], J. Saffer[36], D. Salazar-Gallegos[28], P. Sampathkumar[35], S. E. Sanchez Herrera[28], A. Sandrock[75], P. Sandstrom[47], M. Santander[70], S. Sarkar[29], S. Sarkar[58], J. Savelberg[1], P. Savina[47], M. Schaufel[1], H. Schieler[35], S. Schindler[30], L. Schlickmann[1], B. Schlüter[52], F. Schlüter[12], N. Schmeisser[75], T. Schmidt[23], J. Schneider[30], F. G. Schröder[35, 53], L. Schumacher[30], G. Schwefer[1], S. Sclafani[23], D. Seckel[53], M. Seikh[40], S. Seunarine[62], M. H. Shaevitz[55], R. Shah[60], A. Sharma[74], S. Shefali[36], N. Shimizu[16], M. Silva[47], B. Skrzypek[14], D. Smith[19, 21], B. Smithers[4], R. Snihur[47], J. Soedingrekso[27], A. Søgaard[26], D. Soldin[36], P. Soldin[1], G. Sommani[11], D. Southall[19, 21], C. Spannfellner[31], G. M. Spiczak[62], C. Spiering[76], M. Stamatikos[25], T. Stanev[53], T. Stezelberger[9], J. Stoffels[13], T. Stürwald[75], T. Stuttard[26], G. W. Sullivan[23], I. Taboada[6], A. Taketa[69], H. K. M. Tanaka[69], S. Ter-Antonyan[7], M. Thiesmeyer[1], W. G. Thompson[14], J. Thwaites[47], S. Tilav[53], K. Tollefson[28], C. Tönnis[67], J. Torres[24, 25], S. Toscano[12], D. Tosi[47], A. Trettin[76], Y. Tsunesada[57], C. F. Tung[6], R. Turcotte[35], J. P. Twagirayezu[28], B. Ty[47], M. A. Unland Elorrieta[52], A. K. Upadhyay[47, 77], K. Upshaw[7], N. Valtonen-Mattila[74], J. Vandenbroucke[47], N. van Eijndhoven[13], D. Vannerom[15], J. van Santen[76], J. Vara[52], D. Veberic[35], J. Veitch-Michaelis[47], M. Venugopal[35], S. Verpoest[53], A. Vieregg[18, 19, 20, 21], A. Vijai[23], C. Walck[65], C. Weaver[28], P. Weigel[15], A. Weindl[35], J. Weldert[72], C. Welling[21], C. Wendt[47], J. Werthebach[27], M. Weyrauch[35], N. Whitehorn[28], C. H. Wiebusch[1], N. Willey[28], D. R. Williams[70], S. Wissel[71, 72, 73], L. Witthaus[27], A. Wolf[1], M. Wolf[31], G. Wörner[35], G. Wrede[30], S. Wren[49], X. W. Xu[7], J. P. Yanez[29], E. Yildizci[47], S. Yoshida[16], R. Young[40], F. Yu[14], S. Yu[28], T. Yuan[47], Z. Zhang[66], P. Zhelnin[14], S. Zierke[1], M. Zimmerman[47]

[1] III. Physikalisches Institut, RWTH Aachen University, D-52056 Aachen, Germany
[2] Department of Physics, University of Adelaide, Adelaide, 5005, Australia
[3] Dept. of Physics and Astronomy, University of Alaska Anchorage, 3211 Providence Dr., Anchorage, AK 99508, USA
[4] Dept. of Physics, University of Texas at Arlington, 502 Yates St., Science Hall Rm 108, Box 19059, Arlington, TX 76019, USA
[5] CTSPS, Clark-Atlanta University, Atlanta, GA 30314, USA
[6] School of Physics and Center for Relativistic Astrophysics, Georgia Institute of Technology, Atlanta, GA 30332, USA

[7] Dept. of Physics, Southern University, Baton Rouge, LA 70813, USA
[8] Dept. of Physics, University of California, Berkeley, CA 94720, USA
[9] Lawrence Berkeley National Laboratory, Berkeley, CA 94720, USA
[10] Institut für Physik, Humboldt-Universität zu Berlin, D-12489 Berlin, Germany
[11] Fakultät für Physik & Astronomie, Ruhr-Universität Bochum, D-44780 Bochum, Germany
[12] Université Libre de Bruxelles, Science Faculty CP230, B-1050 Brussels, Belgium
[13] Vrije Universiteit Brussel (VUB), Dienst ELEM, B-1050 Brussels, Belgium
[14] Department of Physics and Laboratory for Particle Physics and Cosmology, Harvard University, Cambridge, MA 02138, USA
[15] Dept. of Physics, Massachusetts Institute of Technology, Cambridge, MA 02139, USA
[16] Dept. of Physics and The International Center for Hadron Astrophysics, Chiba University, Chiba 263-8522, Japan
[17] Department of Physics, Loyola University Chicago, Chicago, IL 60660, USA
[18] Dept. of Astronomy and Astrophysics, University of Chicago, Chicago, IL 60637, USA
[19] Dept. of Physics, University of Chicago, Chicago, IL 60637, USA
[20] Enrico Fermi Institute, University of Chicago, Chicago, IL 60637, USA
[21] Kavli Institute for Cosmological Physics, University of Chicago, Chicago, IL 60637, USA
[22] Dept. of Physics and Astronomy, University of Canterbury, Private Bag 4800, Christchurch, New Zealand
[23] Dept. of Physics, University of Maryland, College Park, MD 20742, USA
[24] Dept. of Astronomy, Ohio State University, Columbus, OH 43210, USA
[25] Dept. of Physics and Center for Cosmology and Astro-Particle Physics, Ohio State University, Columbus, OH 43210, USA
[26] Niels Bohr Institute, University of Copenhagen, DK-2100 Copenhagen, Denmark
[27] Dept. of Physics, TU Dortmund University, D-44221 Dortmund, Germany
[28] Dept. of Physics and Astronomy, Michigan State University, East Lansing, MI 48824, USA
[29] Dept. of Physics, University of Alberta, Edmonton, Alberta, Canada T6G 2E1
[30] Erlangen Centre for Astroparticle Physics, Friedrich-Alexander-Universität Erlangen-Nürnberg, D-91058 Erlangen, Germany
[31] Technical University of Munich, TUM School of Natural Sciences, Department of Physics, D-85748 Garching bei München, Germany
[32] Département de physique nucléaire et corpusculaire, Université de Genève, CH-1211 Genève, Switzerland
[33] Dept. of Physics and Astronomy, University of Gent, B-9000 Gent, Belgium
[34] Dept. of Physics and Astronomy, University of California, Irvine, CA 92697, USA
[35] Karlsruhe Institute of Technology, Institute for Astroparticle Physics, D-76021 Karlsruhe, Germany
[36] Karlsruhe Institute of Technology, Institute of Experimental Particle Physics, D-76021 Karlsruhe, Germany
[37] Dept. of Physics, Engineering Physics, and Astronomy, Queen's University, Kingston, ON K7L 3N6, Canada
[38] Department of Physics & Astronomy, University of Nevada, Las Vegas, NV, 89154, USA
[39] Nevada Center for Astrophysics, University of Nevada, Las Vegas, NV 89154, USA
[40] Dept. of Physics and Astronomy, University of Kansas, Lawrence, KS 66045, USA
[41] Dept. of Physics and Astronomy, University of Nebraska–Lincoln, Lincoln, Nebraska 68588, USA
[42] Dept. of Physics, King's College London, London WC2R 2LS, United Kingdom
[43] School of Physics and Astronomy, Queen Mary University of London, London E1 4NS, United Kingdom
[44] Centre for Cosmology, Particle Physics and Phenomenology - CP3, Université catholique de Louvain, Louvain-la-Neuve, Belgium
[45] Department of Physics, Mercer University, Macon, GA 31207-0001, USA
[46] Dept. of Astronomy, University of Wisconsin–Madison, Madison, WI 53706, USA
[47] Dept. of Physics and Wisconsin IceCube Particle Astrophysics Center, University of Wisconsin–Madison, Madison, WI 53706, USA
[48] Institute of Physics, University of Mainz, Staudinger Weg 7, D-55099 Mainz, Germany
[49] School of Physics and Astronomy, The University of Manchester, Oxford Road, Manchester, M13 9PL, United Kingdom
[50] Department of Physics, Marquette University, Milwaukee, WI, 53201, USA
[51] Dept. of High Energy Physics, Tata Institute of Fundamental Research, Colaba, Mumbai 400 005, India
[52] Institut für Kernphysik, Westfälische Wilhelms-Universität Münster, D-48149 Münster, Germany
[53] Bartol Research Institute and Dept. of Physics and Astronomy, University of Delaware, Newark, DE 19716, USA
[54] Dept. of Physics, Yale University, New Haven, CT 06520, USA
[55] Columbia Astrophysics and Nevis Laboratories, Columbia University, New York, NY 10027, USA
[56] Dept. of Physics, University of Notre Dame du Lac, 225 Nieuwland Science Hall, Notre Dame, IN 46556-5670, USA
[57] Graduate School of Science and NITEP, Osaka Metropolitan University, Osaka 558-8585, Japan
[58] Dept. of Physics, University of Oxford, Parks Road, Oxford OX1 3PU, United Kingdom
[59] Dipartimento di Fisica e Astronomia Galileo Galilei, Università Degli Studi di Padova, 35122 Padova PD, Italy
[60] Dept. of Physics, Drexel University, 3141 Chestnut Street, Philadelphia, PA 19104, USA
[61] Physics Department, South Dakota School of Mines and Technology, Rapid City, SD 57701, USA
[62] Dept. of Physics, University of Wisconsin, River Falls, WI 54022, USA
[63] Dept. of Physics and Astronomy, University of Rochester, Rochester, NY 14627, USA
[64] Department of Physics and Astronomy, University of Utah, Salt Lake City, UT 84112, USA
[65] Oskar Klein Centre and Dept. of Physics, Stockholm University, SE-10691 Stockholm, Sweden
[66] Dept. of Physics and Astronomy, Stony Brook University, Stony Brook, NY 11794-3800, USA
[67] Dept. of Physics, Sungkyunkwan University, Suwon 16419, Korea

[68] Institute of Physics, Academia Sinica, Taipei, 11529, Taiwan
[69] Earthquake Research Institute, University of Tokyo, Bunkyo, Tokyo 113-0032, Japan
[70] Dept. of Physics and Astronomy, University of Alabama, Tuscaloosa, AL 35487, USA
[71] Dept. of Astronomy and Astrophysics, Pennsylvania State University, University Park, PA 16802, USA
[72] Dept. of Physics, Pennsylvania State University, University Park, PA 16802, USA
[73] Institute of Gravitation and the Cosmos, Center for Multi-Messenger Astrophysics, Pennsylvania State University, University Park, PA 16802, USA
[74] Dept. of Physics and Astronomy, Uppsala University, Box 516, S-75120 Uppsala, Sweden
[75] Dept. of Physics, University of Wuppertal, D-42119 Wuppertal, Germany
[76] Deutsches Elektronen-Synchrotron DESY, Platanenallee 6, 15738 Zeuthen, Germany
[77] Institute of Physics, Sachivalaya Marg, Sainik School Post, Bhubaneswar 751005, India
[78] Department of Space, Earth and Environment, Chalmers University of Technology, 412 96 Gothenburg, Sweden
[79] Earthquake Research Institute, University of Tokyo, Bunkyo, Tokyo 113-0032, Japan

Acknowledgements

The authors gratefully acknowledge the support from the following agencies and institutions: USA – U.S. National Science Foundation-Office of Polar Programs, U.S. National Science Foundation-Physics Division, U.S. National Science Foundation-EPSCoR, Wisconsin Alumni Research Foundation, Center for High Throughput Computing (CHTC) at the University of Wisconsin–Madison, Open Science Grid (OSG), Advanced Cyberinfrastructure Coordination Ecosystem: Services & Support (ACCESS), Frontera computing project at the Texas Advanced Computing Center, U.S. Department of Energy-National Energy Research Scientific Computing Center, Particle astrophysics research computing center at the University of Maryland, Institute for Cyber-Enabled Research at Michigan State University, and Astroparticle physics computational facility at Marquette University; Belgium – Funds for Scientific Research (FRS-FNRS and FWO), FWO Odysseus and Big Science programmes, and Belgian Federal Science Policy Office (Belspo); Germany – Bundesministerium für Bildung und Forschung (BMBF), Deutsche Forschungsgemeinschaft (DFG), Helmholtz Alliance for Astroparticle Physics (HAP), Initiative and Networking Fund of the Helmholtz Association, Deutsches Elektronen Synchrotron (DESY), and High Performance Computing cluster of the RWTH Aachen; Sweden – Swedish Research Council, Swedish Polar Research Secretariat, Swedish National Infrastructure for Computing (SNIC), and Knut and Alice Wallenberg Foundation; European Union – EGI Advanced Computing for research; Australia – Australian Research Council; Canada – Natural Sciences and Engineering Research Council of Canada, Calcul Québec, Compute Ontario, Canada Foundation for Innovation, WestGrid, and Compute Canada; Denmark – Villum Fonden, Carlsberg Foundation, and European Commission; New Zealand – Marsden Fund; Japan – Japan Society for Promotion of Science (JSPS) and Institute for Global Prominent Research (IGPR) of Chiba University; Korea – National Research Foundation of Korea (NRF); Switzerland – Swiss National Science Foundation (SNSF); United Kingdom – Department of Physics, University of Oxford.